CONF-781202--3

DP-MS-78-14

MASTER

NUMERICAL SOLUTION OF THREE-DIMENSIONAL NATURAL CONVECTION BY THE STRONGLY IMPLICIT PROCEDURE

D. W. Pepper (Research Engineer; Member ASME)
S. D. Harris (Research Supervisor; Member ASME)

Savannah River Laboratory
E. I. du Pont de Nemours and Company
Aiken, South Carolina 29801

Paper for presentation at the
1978 Winter Annual Meeting of ASME
Session on Heat Transfer in Enclosures
San Francisco, California
December 10-15, 1978

This paper was prepared in connection with work under Contract No. AT(07-2)-1 with the U. S. Department of Energy.

DISCLAIMER

NUMERICAL SOLUTION OF THREE-DIMENSIONAL NATURAL CONVECTION BY THE STRONGLY IMPLICIT PROCEDURE

D. W. PEPPER (Research Engineer; Member ASME)
S. D. HARRIS (Research Supervisor; Member ASME)

Savannah River Laboratory
E. I. du Pont de Nemours and Company
Aiken, South Carolina 29801

ABSTRACT

A numerical model has been developed to solve three-dimensional laminar flow in enclosures. The model is based on a three-dimensional strongly implicit procedure (SIP). In simple cases of natural convection due to differential side heating, numerical results at low and moderate Rayleigh numbers agree with results appearing in the literature. Although the model requires a moderate amount of computer storage, computation times are relatively fast. The simple case of heating a cubical room by a uniform floor or ceiling heat system with a vertical wall exposed to a uniformly cooled surface is also investigated.

INTRODUCTION

The strongly implicit procedure (SIP), first developed by Stone [1],[1] has been used predominantly to calculate two-dimensional viscous flow problems. Bozeman and Dalton [2] used SIP to calculate two-dimensional viscous flow in a cavity and obtained stable solutions up to Reynolds number = 1000. Jacobs [3] has obtained stable flow solutions at high Reynolds numbers with an SIP-upwind differencing scheme. The flow over a circular cylinder was calculated by Lin et al. [4] with SIP, an ADIP (alternating direction implicit procedure), and an upwind differencing scheme. Computation times and accuracy with known experimental results were compared; SIP was found to give accurate results in less computation time than the other two methods. Pepper and Harris [5,6] calculated natural convection in closed containers with an alternating SIP and obtained solutions up to Rayleigh numbers $\sim 10^6$.

[1] Numbers in brackets designate References at end of paper.

Application of SIP to three-dimensional problems has been limited. The three-dimensional algorithms were initially developed by Weinstein et al. [7] to calculate multiphase reservoir flow problems. However, three-dimensional SIP has been used by Long and Pepper [8] and Pepper and Kern [9] to calculate time-dependent mesoscale transport of concentration.

Three-dimensional problems are considerably more difficult to solve than two-dimensional problems because the number of unknown transport terms to be solved is increased, and because a more complicated set of boundary constraints (Ozoe et al. [10]) must be used. Numerical instability and time and memory requirements are also more severe. The SIP method appears to be a reliable computational scheme which can alleviate some of these restrictions.

Natural convection problems have been successfully analyzed by several investigators with three-dimensional numerical techniques. Aziz and Hellums [11] used a three-dimensional ADIP with a Crank-Nicolson procedure to calculate natural convection in an enclosure with heating from below. Solutions were obtained with the vorticity-vector potential equations and with the three-dimensional equations of motion. Best results were obtained with the vorticity-vector potential form of the governing equations. Williams [12] used Dufort-Frankel differencing to solve the equations of motion for free convection in an annular space and obtained satisfactory results, but significant amounts of computation time were required. Holst and Aziz [13] calculated transient natural convection in porous media with ADIP and SOR (successive over-relaxation) procedures to solve the set of vorticity-vector potential equations. Higher heat transfer rates occurred across porous media in three-dimensional

motion than in two-dimensional motion. Lipps [14] has also calculated three-dimensional Bénard convection based on the numerical method used by Williams [12].

Mallinson and de Vahl Davis [15] calculated three-dimensional laminar natural convection in an enclosure with ADIP coupled with a false transient procedure to convert the steady state vector potential equations to parabolic form. This procedure created a marching solution equivalent to a single iterative procedure for the vector potential equations. Mallinson and de Vahl Davis [15] found the vorticity-vector potential form of the governing equations to be best suited for calculating three-dimensional free convective flow in an enclosure. Ozoe et al. [10] used ADIP to calculate the three-dimensional vorticity-vector potential equations for natural convection with heating from below in a cubical box, a long channel, and the region between infinite, horizontal plates. Numerical results agreed with experimental results. Ozoe et al. [10] also obtained realistic results for natural convection in a long inclined rectangular box heated from below.

ADIP is normally used to calculate three-dimensional equations. However, ADIP requires a splitting of the time step along with a triple sweep of the solution domain to obtain the three-dimensional values of one field variable. Although only a tridiagonal is solved per sweep, the solution time increases significantly as the number of equations increases. SIP solves the unknown variables without requiring a splitting of the time step and yet still solves the three-dimensional implicit form of the equation with efficient matrix solution algorithms. In many instances, SIP has been found to be more accurate and less time consuming than ADIP (Stone et al. [1] and Lin et al. [4]).

To assess the computational model, several simple test cases are analyzed for three-dimensional, laminar, natural convection in an enclosed fluid with constant properties. Differential side heating is used with one vertical wall heated and the opposite wall cooled. The top, bottom, and remaining side vertical walls are insulated. The temperature gradients created by these boundary conditions influence buoyancy, which causes the fluid to rotate.

A simple case of interest in comfort heating is also analyzed: heating of a cubical room by a uniform floor or ceiling "radiant" heat system. The system is modeled by assuming that a vertical wall is exposed to a cooled surface at constant temperature. Interior side and rear walls are insulated. In one case, the floor is heated at constant temperature (e.g., by a hydronic system with inlaid pipes, or by an electrical system with imbedded heating cables), and the ceiling is insulated. For the other case, the inverse system is assumed with the ceiling heated and the floor insulated. The question of which system produces more comfortable air temperatures and uniform air patterns minimizing drafts is briefly examined.

GOVERNING EQUATIONS

The equations of motion for laminar natural convection in an enclosure can be written in nondimensional form [10,15] as

$$\frac{\partial \vec{\omega}}{\partial \tau} = \nabla\times(\vec{\omega}\times\vec{U}) - PrRa\ (\nabla\times\theta\vec{g}) + Pr\nabla^2\vec{\omega} \qquad (1)$$

$$0 = \nabla^2\vec{\Psi} + \vec{\omega} \qquad (2)$$

$$\frac{\partial \theta}{\partial \tau} = -\nabla\cdot(\vec{U}\theta) + \nabla^2\theta \qquad (3)$$

where $\vec{\omega}$ is the vorticity vector, $\vec{\Psi}$ is the vector potential, θ is the temperature, $\vec{U}$ is the velocity vector, and $\vec{g}$ is the gravitational vector.

The equation set is written in divergence form in order to permit the velocity-vorticity products to be evaluated at the same point (conserving vorticity in a local sense). Bozeman and Dalton [2] found that the divergence form of the two-dimensional vorticity transport equation gave more reliable results with SIP than with the convective form.

Equations (1) through (3) are based on the premise that $\nabla\cdot\vec{U} = 0$. In actuality, equation (2) can be rewritten as $\vec{\omega} = -\nabla^2\vec{\Psi} + \nabla(\nabla\cdot\vec{\Psi})$. Assuming incompressibility, the vector potential in the exact solution is solenoidal. However, since the numerical solution is inexact, $\nabla\cdot\vec{U}$ will have some nonzero value. However, Aziz and Hellums [11] found that $\nabla(\nabla\cdot\vec{\Psi})$ for a $10 \times 10 \times 10$ mesh was negligible compared to $\nabla^2\vec{\Psi}$. In an effort to numerically determine how well divergence is satisfied within the computational domain, $\nabla\cdot\vec{U}$ was calculated throughout the enclosure.[2] Maximum values did not exceed 10^{-2} for cases where $10^4 \le Ra \le 10^5$.

To enhance the rate of transient convergence, equations (1) and (2) are altered to the following form [15]:

$$\frac{Pr}{\alpha_w}\frac{\partial \vec{\omega}}{\partial \tau} = -\nabla\times(\vec{\omega}\times\vec{U}) - PrRa\ (\nabla\times\theta\vec{g}) + Pr\nabla^2\vec{\omega} \qquad (4)$$

$$\frac{1}{\alpha_\psi}\frac{\partial \vec{\Psi}}{\partial \tau} = \nabla^2\vec{\Psi} + \vec{\omega} \qquad (5)$$

$$\frac{\partial \theta}{\partial \tau} = -\nabla\cdot(\vec{U}\theta) + \nabla^2\theta \qquad (6)$$

where the transient term in equation (1) is premultiplied by (Pr/α_w) and a fictitious transient term added to equation (2). Parameters α_w and α_ψ are set equal for 0.050 and 1.0, respectively. Although the true transient solutions are lost, the solutions behave similarly to the transient nature of the flow. At long periods of time, the transient terms become insignificant and the true steady-state solution is obtained.

The vorticity vector and the vector potential can be written in terms of three-dimensional components as

$$\vec{\omega} = w_1\hat{i} + w_2\hat{j} + w_3\hat{k} \text{ and } \vec{\Psi} = \Psi_1\hat{i} + \Psi_2\hat{j} + \Psi_3\hat{k} \qquad (7)$$

Subscripts 1, 2, and 3 denote values in the X, Y, and Z planes, respectively. The three-dimensional region is confined by the planes X = 0,1, Y = 0,1, and Z = 0,1 as shown in Figure 1.

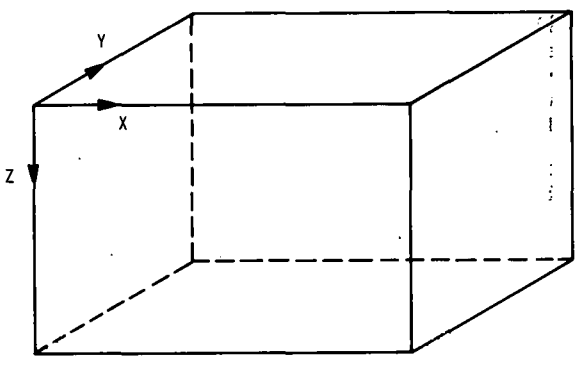

Fig. 1 Three-dimensional solution domain

[2] A fourth order three-dimensional cubic spline technique was used to calculate the first order gradients (Rubin et al. [19]).

The boundary conditions subject to solution of equations (4) through (6) are given in Table 1. Formulation of the boundary conditions are discussed by Hirasaki and Hellums [17], Mallinson and de Vahl Davis [15], and Aziz and Hellums [11]. Finite difference approximations to the boundary condition relation for $\bar{\Psi}$ and θ are based on three point central difference approximations and imaginary points outside the solution domain. Vorticity boundary conditions are approximated by assuming vorticity to vary linearly with wall distance (Gosman et al. [18]). In order to enhance stabilization of the computation, the wall vorticity values are weight-averaged with both old and new values such that

$$\vec{\omega}^{n+1} = (1-\gamma)\ \vec{\omega}^{n}\big|_{wall} + \gamma\vec{\omega}^{*}\big|_{wall} \qquad (8)$$

where ω^* is calculated from the most recent vorticity boundary condition relation and γ is the weight-averaged coefficient. Best results were obtained with $\gamma = 0.6$, as in Reference [2].

Table 1. Boundary conditions

	X = 0,1	Y = 0,1	Z = 0,1
ω_1	0	$-\frac{\partial^2\Psi_1}{\partial Y^2}$	$-\frac{\partial^2\Psi_1}{\partial Z^2}$
ω_2	$-\frac{\partial^2\Psi_2}{\partial X^2}$	0	$-\frac{\partial^2\Psi_2}{\partial Z^2}$
ω_3	$\frac{\partial^2\Psi_3}{\partial X^2}$	$\frac{\partial^2\Psi_3}{\partial Y^2}$	0
Ψ_1	$\frac{\partial\Psi_1}{\partial X} = 0$	0	0
Ψ_2	0	$\frac{\partial\Psi_2}{\partial Y} = 0$	0
Ψ_3	0	0	$\frac{\partial\Psi_3}{\partial Z} = 0$
T (side heating)	1,0	$\frac{\partial T}{\partial Y} = 0$	$\frac{\partial T}{\partial Z} = 0$
T (heating from above, below)	$\frac{\partial T}{\partial X} = 0,0$	$\frac{\partial T}{\partial Y} = 0$	$T = 1,\ \frac{\partial T}{\partial Z} = 0$ $\frac{\partial T}{\partial Z} = 0,\ T = 1$

NUMERICAL METHOD

SIP requires the equations of motion to be separated into discrete finite differences by forward-in-time, centered-in-space approximations for the derivative terms. This discretization creates a sparse matrix banded by seven diagonal elements. SIP alters this matrix into a series of upper and lower matrices, which can be solved efficiently by Gaussian elimination techniques. The discretized form of equation (4) for the ω_1 component vorticity is written as

$$\frac{Pr}{\alpha_\omega}\frac{\omega_{1_{i,j,k}}^{n+1} - \omega_{1_{i,j,k}}^{n}}{\Delta\tau} - \frac{V_{i,j+1,k}^{n}\omega_{1_{i,j+1,k}}^{n+1} - V_{i,j-1,k}^{n}\omega_{1_{i,j-1,k}}^{n+1}}{2\Delta Y} - \frac{W_{i,j,k+1}\omega_{1_{i,j,k+1}}^{n+1} - W_{i,j,k-1}\omega_{1_{i,j,k-1}}^{n+1}}{2\Delta Z}$$

$$+ \frac{U_{i,j+1,k}\omega_{2_{i,j+1,k}}^{n} - U_{i,j-1,k}\omega_{2_{i,j-1,k}}^{n}}{2\Delta Y} + \frac{U_{i,j,k+1}\omega_{3_{i,j,k+1}}^{n} - U_{i,j,k-1}\omega_{3_{i,j,k-1}}^{n}}{2\Delta Z}$$

$$- RaPr\frac{(\theta_{i,j+1,k}^{n} - \theta_{i,j-1,k}^{n})}{2\Delta Y} + Pr\left[\frac{\omega_{1_{i+1,j,k}}^{n+1} - 2\omega_{1_{i,j,k}}^{n+1} + \omega_{1_{i-1,j,k}}^{n+1}}{\Delta X^2} + \frac{\omega_{1_{i,j+1,k}}^{n+1} - 2\omega_{1_{i,j,k}}^{n+1} + \omega_{1_{i,j-1,k}}^{n+1}}{\Delta Y^2} + \frac{\omega_{1_{i,j,k+1}}^{n+1} - 2\omega_{1_{i,j,k}}^{n+1} + \omega_{1_{i,j,k-1}}^{n+1}}{\Delta Z^2}\right] \qquad (9)$$

Similar relations can be written for the ω_2, ω_3, $\bar{\Psi}_{1-3}$, and θ equations. The advection terms in equation (9) have been written in conservative form to ensure conservation of vorticity in the finite difference form as well as in the differential form. A finite difference molecule for equation (9) is shown in Figure 2. Equation (9) can be rewritten as

$$D_{i,j,k}\omega_{1_{i-1,j,k}}^{n+1} + F_{i,j,k}\omega_{1_{i+1,j,k}}^{n+1} + B_{i,j,k}\omega_{1_{i,j-1,k}}^{n+1} + H_{i,j,k}\omega_{1_{i,j+1,k}}^{n+1} + Z'_{i,j,k}\omega_{1_{i,j,k-1}}^{n+1} + S_{i,j,k}\omega_{1_{i,j,k+1}}^{n+1} + E_{i,j,k}\omega_{1_{i,j,k}}^{n+1} = q_{i,j,k}^{n} \qquad (10)$$

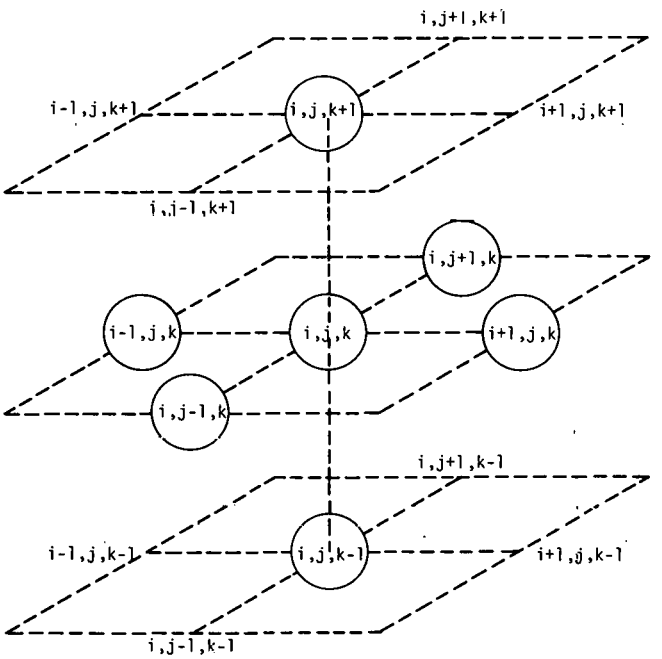

Fig. 2 Computational grid molecule

Coefficients $D_{i,j,k}$, $F_{i,j,k}$, $B_{i,j,k}$, $H_{i,j,k}$, $Z'_{i,j,k}$, $S_{i,j,k}$, and $E_{i,j,k}$ and their subsequent values for the remaining equations in the set are defined in Table 2.

Table 2. Coefficients of [M]

	ω_1	ω_2	ω_3	Ψ_1, Ψ_2, Ψ_3	T
D_i	$-Pr/\Delta X^2$	$-\frac{U_{i-1,j,k}}{2\Delta X} - \frac{Pr}{\Delta X^2}$	$-\frac{U_{i-1,j,k}}{2\Delta X} - \frac{Pr}{\Delta X^2}$	$-1/\Delta X^2$	$-\frac{U_{i-1,j,k}}{2\Delta X} - \frac{1}{\Delta X^2}$
F_i	$-Pr/\Delta X^2$	$\frac{U_{i+1,j,k}}{2\Delta X} - \frac{Pr}{\Delta X^2}$	$\frac{U_{i+1,j,k}}{2\Delta X} - \frac{Pr}{\Delta X^2}$	$-1/\Delta X^2$	$\frac{U_{i+1,j,k}}{2\Delta X} - \frac{1}{\Delta X^2}$
B_i	$-\frac{V_{i,j-1,k}}{2\Delta Y} - Pr/\Delta Y^2$	$-\frac{Pr}{\Delta Y^2}$	$-\frac{V_{i,j-1,k}}{2\Delta Y} - \frac{Pr}{\Delta Y^2}$	$-1/\Delta Y^2$	$-\frac{V_{i,j-1,k}}{2\Delta Y} - \frac{1}{\Delta Y^2}$
H_i	$\frac{V_{i,j+1,k}}{2\Delta Y} - \frac{Pr}{\Delta Y^2}$	$-\frac{Pr}{\Delta Y^2}$	$\frac{V_{i,j+1,k}}{2\Delta Y} - \frac{Pr}{\Delta Y^2}$	$-1/\Delta Y^2$	$\frac{V_{i,j+1,k}}{2\Delta Y} - \frac{1}{\Delta Y^2}$
Z'_i	$-\frac{W_{i,j,k-1}}{2\Delta Z} - \frac{Pr}{\Delta Z^2}$	$-\frac{W_{i,j,k+1}}{2\Delta Z} - \frac{Pr}{\Delta Z^2}$	$-\frac{Pr}{\Delta Z^2}$	$-1/\Delta Z^2$	$-\frac{W_{i,j,k-1}}{2\Delta Z} - \frac{1}{\Delta Z^2}$
S_i	$\frac{W_{i,j,k+1}}{2\Delta Z} - \frac{Pr}{\Delta Z^2}$	$\frac{W_{i,j,k+1}}{2\Delta Z} - \frac{Pr}{\Delta Z^2}$	$-\frac{Pr}{\Delta Z^2}$	$-1/\Delta Z^2$	$\frac{W_{i,j,k+1}}{2\Delta Z} - \frac{1}{\Delta Z^2}$
E_i	$\frac{Pr}{\alpha_\omega \Delta\tau} + \frac{2Pr}{\Delta X^2} + \frac{2Pr}{\Delta Y^2} + \frac{2Pr}{\Delta Z^2}$			$\frac{1}{\alpha_s \Delta\tau} + \frac{2}{\Delta X^2} + \frac{2}{\Delta Y^2} + \frac{2}{\Delta Z^2}$	$\frac{1}{\Delta\tau} + \frac{2}{\Delta X^2} + \frac{2}{\Delta Y^2} + \frac{2}{\Delta Z^2}$

Equation (10) can be rewritten in matrix form as

$$[M]\{\phi\} = \{q\} \tag{11}$$

where [M] is the sparse coefficient matrix containing seven diagonals, $\{\phi\}$ is the column matrix of unknown values of vorticity, vector potentials, or temperature. $\{q\}$ is the column matrix of explicitly known values evaluated at the nth time step. The coefficients of $\{q\}$ are shown in Table 3.

Table 3. Coefficients of $\{q\}$

	q_i^n
ω_1	$\phi_{i,j,k}\frac{Pr}{\alpha_\omega\Delta\tau} + \frac{U_{i,j+1,k}\omega 2_{i,j+1,k} - U_{i,j-1,k}\omega 2_{i,j-1,k}}{2\Delta Y} + \frac{U_{i,j,k+1}\omega 3_{i,j,k+1} - U_{i,j,k-1}\omega 3_{i,j,k-1}}{2\Delta Z} + PrRa\frac{\theta_{i,j+1,k} - \theta_{i,j-1k}}{2\Delta Y}$
ω_2	$\phi_{i,j,k}\frac{Pr}{\alpha_\omega\Delta\tau} + \frac{V_{i+1,j,k}\omega 1_{i+1,j,k} - V_{i-1,j,k}\omega 1_{i-1,j,k}}{2\Delta X} + \frac{V_{i,j,k+1}\omega 3_{i,j,k+1} - V_{i,j,k-1}\omega 3_{i,j,k-1}}{2\Delta Z} + PrRa\frac{\theta_{i+1,j,k} - \theta_{i-1,j,k}}{2\Delta X}$
ω_3	$\phi_{i,j,k}\frac{Pr}{\alpha_\omega\Delta\tau} + \frac{W_{i+1,j,k}\omega 1_{i+1,j,k} - W_{i-1,j,k}\omega 1_{i-1,j,k}}{2\Delta X} + \frac{W_{i,j+1,k}\omega 2_{i,j+1,k} - W_{i,j-1,k}\omega 2_{i,j-1,k}}{2\Delta Y}$
Ψ_1	$\omega 1_{i,j,k} + \frac{\phi_{i,j,k}}{\alpha_s\Delta\tau}$
Ψ_2	$\omega 2_{i,j,k} + \frac{\phi_{i,j,k}}{\alpha_s\Delta\tau}$
Ψ_3	$\omega 3_{i,j,k} + \frac{\phi_{i,j,k}}{\alpha_s\Delta\tau}$
θ	$\frac{\phi_{i,j,k}}{\Delta\tau}$

In order to efficiently solve matrix [M], equation (9) is altered by adding additional terms similar to the procedure used in two-dimensional SIP. This alteration allows matrix [M] to be factored into lower and upper matrices, [Ld] and [Ud], which require less computer storage and calculation time when solved by elimination techniques. Equation (9) is rewritten as

$$\begin{aligned}
&D_{i,j,k}\phi_{i-1,j,k} + B_{i,j,k}\phi_{i,j-1,k} + Z'_{i,j,k}\phi_{i,j,k-1} \\
&+ E_{i,j,k}\phi_{i,j,k} + F_{i,j,k}\phi_{i+1,j,k} + H_{i,j,k}\phi_{i,j+1,k} \\
&+ S_{i,j,k}\phi_{i,j,k+1} + C_{i,j,k}[\phi_{i+1,j-1,k} - \alpha_1(-\phi_{i,j,k} \\
&+ \phi_{i+1,j,k} + \phi_{i,j-1,k})] + G_{i,j,k}[\phi_{i-1,j+1,k} \\
&- \alpha_1(-\phi_{i,j,k} + \phi_{i-1,j,k} + \phi_{i,j+1,k})] \\
&+ A_{i,j,k}[\phi_{i+1,j,k-1} - \alpha_2(-\phi_{i,j,k} + \phi_{i+1,j,k} + \phi_{i,j,k-1})] \\
&+ W'_{i,j,k}[\phi_{i-1,j,k+1} - \alpha_2(-\phi_{i,j,k} + \phi_{i-1,j,k} + \phi_{i,j,k+1})] \\
&+ T'_{i,j,k}[\phi_{i,j+1,k-1} - \alpha_3(-\phi_{i,j,k} + \phi_{i,j+1,k} + \phi_{i,j,k-1})] \\
&+ P_{i,j,k}[\phi_{i,j-1,k+1} - \alpha_3(-\phi_{i,j,k} + \phi_{i,j-1,k} + \phi_{i,j,k+1})] \\
&= R_{i,j,k}
\end{aligned} \tag{12}$$

The first seven terms on the left-hand side of equation (12) are the original coefficients of equation (9); the remaining terms, $C_{i,j,k}$, $G_{i,j,k}$, $A_{i,j,k}$, $W'_{i,j,k}$, $T'_{i,j,k}$, and $P_{i,j,k}$ are coefficients associated with the additional new unknown values $\phi_{i+1,j-1,k}$, $\phi_{i-1,j+1,k}$, $\phi_{i+1,j,k-1}$, $\phi_{i,j+1,k-1}$, and $\phi_{i,j-1,k+1}$, respectively. The influence of these new terms is reduced by subtracting nearly equal terms (in parentheses) adjacent to the new variables. The parameters α_1, α_2, and α_3 are iteration values which

vary between $0 < \alpha_i < 1$ to account for large variations in $\phi_{i,j,k}$ or variable grid spacing. A cyclic set of ten values for α_i was used based on the procedure described by Weinstein et al. [7].

Equation (12) can be written in matrix notation as

$$[M']\{\phi\} = \{q\} \tag{13}$$

[M'] now contains 13 diagonal coefficients. Factorizing [M'] into the product of upper and lower matrices creates two matrices each containing four nonzero diagonal elements. Figure 3 shows the original seven-diagonal matrix, and Figure 4 shows the altered matrix with the [Ud] and [Ld] matrices.

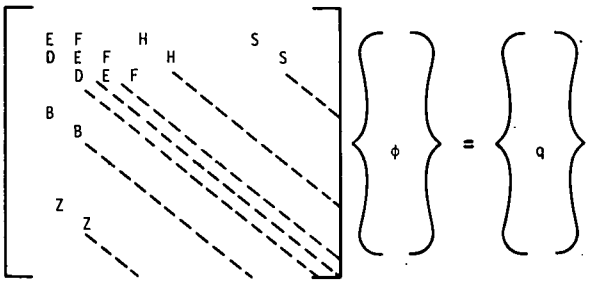

Fig. 3 Original seven-diagonal matrix [M]

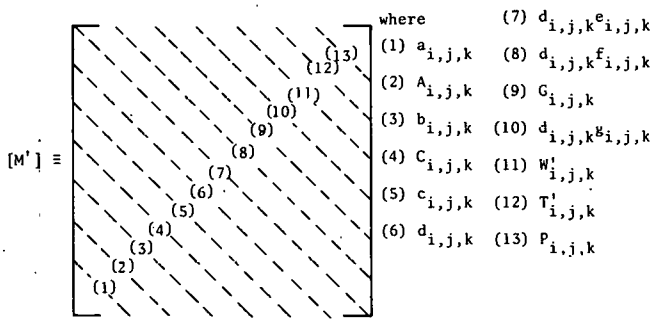

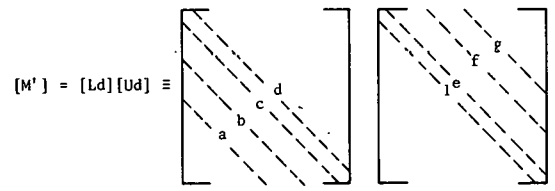

Fig. 4 Altered coefficient of [M']

The three-dimensional SIP algorithms are based on the [Ld] and [Ud] diagonal terms and are given as

$$a_{i,j,k} = Z'_{i,j,k}/(1 + \alpha_2 e_{i,j,k-1} + \alpha_1 f_{i,j,k-1})$$

$$b_{i,j,k} = B_{i,j,k}/(1 + \alpha_2 g_{i,j-1,k} + \alpha_1 e_{i,j-1,k})$$

$$c_{i,j,k} = D_{i,j,k}/(1 + \alpha_2 g_{i-1,j,k} + \alpha_1 f_{i-1,j,k})$$

$$A_{i,j,k} = a_{i,j,k} e_{i,j,k-1}$$

$$C_{i,j,k} = b_{i,j,k} e_{i,j-1,k}$$

$$G_{i,j,k} = c_{i,j,k} f_{i-1,j,k}$$

$$W'_{i,j,k} = c_{i,j,k} g_{i-1,j,k}$$

$$T'_{i,j,k} = a_{i,j,k} f_{i,j,k-1}$$

$$P_{i,j,k} = b_{i,j,k} g_{i,j-1,k}$$

$$d_{i,j,k} = E_{i,j,k} + \alpha_2(A_{i,j,k} + W'_{i,j,k}) + \alpha_3(T'_{i,j,k} + P_{i,j,k}) + \alpha_2(C_{i,j,k} + G_{i,j,k}) - c_{i,j,k} e_{i-1,j,k} - b_{i,j,k} f_{i,j-1,k} - a_{i,j,k} g_{i,j,k-1}$$

$$c_{i,j,k} = (F_{i,j,k} - \alpha_2 A_{i,j,k} - \alpha_1 C_{i,j,k})/d_{i,j,k}$$

$$f_{i,j,k} = (H_{i,j,k} - \alpha_3 T'_{i,j,k} - \alpha_1 G_{i,j,k})/d_{i,j,k}$$

$$g_{i,j,k} = (S_{i,j,k} - \alpha_2 W'_{i,j,k} - \alpha_3 P_{i,j,k})/d_{i,j,k} \tag{14}$$

To reduce roundoff errors, the unknown $\phi^{n+1}_{i,j,k}$ values are solved in residual form such that

$$[M']\{\Delta\phi^{n+1}\} = \{R\} \tag{15}$$

where $\{R\} = \{q\} - [M]\{q\}$ as given in equation (12) and $\Delta\phi^{n+1} = \phi^{n+1} - \phi^n$. Equation (15) can be rewritten as

$$[M']\{\Delta\phi^{n+1}\} = [Ld][Ud]\{\Delta\phi^{n+1}\} = \{R\} \tag{16}$$

If $[Ud]\{\Delta\phi^{n+1}\} = \{\tilde{V}\}$, equation (16) becomes

$$[Ld]\{\tilde{V}\} = \{R\} \tag{17}$$

At node point i,j,k, equations (16) and (17) can be written as

$$\tilde{V}_{i,j,k} = (R^n_{i,j,k} - c_{i,j,k}\tilde{V}_{i,j,k-1} - b_{i,j,k}\tilde{V}_{i,j-1,k} - c_{i,j,k}\tilde{V}_{i-1,j,k})/d_{i,j,k} \tag{18}$$

and

$$\Delta\phi^{n+1}_{i,j,k} = \tilde{V}^{n+1}_{i,j,k} - c_{i,j,k}\Delta\phi^{n+1}_{i+1,j,k} - f_{i,j,k}\Delta\phi^{n+1}_{i,j+1,k} - g_{i,j,k}\Delta\phi^{n+1}_{i,j,k+1} \tag{19}$$

Once $\Delta\phi^{n+1}_{i,j,k}$ is solved, $\phi^{n+1}_{i,j,k}$ can be found. An alternate set of algorithms can be written for odd-numbered time steps (or iterations) similar to the procedure outlined by Pepper and Harris [6] and Weinstein et al. [7]. In some instances an alternating sequence may accelerate convergence and maintain stability of the solution by creating overall symmetry in [M']. In this study, the use of an alternating sequence did not enhance the solution time or accuracy; results shown in this analysis are based on the single set algorithms as presented here. In comparing the accuracy of SIP with ADIP, Weinstein et al. [7] found that single precision SIP solutions were comparable to double precision ADIP solutions; that SIP was less sensitive to rounding errors than ADIP; and that although SIP required larger iteration time than ADIP, fewer iterations were needed to converge the solution. Similar studies made by Lin et al. [4] and Pepper and Harris [6] support these observations.

RESULTS

Side Heating

A series of five simple tests was conducted with one vertical side wall heated and the opposite vertical side wall cooled. The Rayleigh numbers were limited to $10^3 \leq Ra \leq 2.5 \times 10^5$ in order to keep computation time to a reasonable level (as well as minimize instability). For low to moderate Rayleigh numbers, steady state results are generally of interest. Solutions beyond $Ra \geq 10^6$ become unsteady and oscillatory (particularly at low Pr), and require more accurate numerical techniques (Fromm [20]).

Steady state results for ω_2, Ψ_2, and θ are shown in Figures 5-7 for Rayleigh numbers 10^3, 10^4, and 10^5, respectively. Contours are drawn in the lateral (Y) plane midway through the enclosure. The aspect ratio is 1(X):1(Y):1(Z), and the Prandtl number is equal to 10. At low to moderate Rayleigh numbers ($10^4 < Ra < 10^5$), the effect of varying Prandtl number on heat transfer rates and flow patterns is minimal. For $Ra \geq 10^5$, changes in Prandtl number dramatically alter temperature flux (and axial flow patterns, [15]). Pr = 10 was chosen in order to compare with results obtained in References [10] and [15] and would be expected to be compatible with results obtained for Pr > 1, providing $Ra < 10^5$. The two-dimensional planar recirculation patterns are similar to two-dimensional patterns obtained in References [11] and [15].[3]

Figure 8 shows steady state results for $Ra = 10^4$ and $Ra = 3 \times 10^4$ with the aspect ratio altered to 1:2:1. The mesh spacing was altered to $11 \times 21 \times 11$. The effect of increasing the longitudinal aspect ratio results in an increase in the strength of the flow; i.e., the maximum Ψ_2 value increases as the aspect ratio is increased; similar effects occur with increasing Rayleigh number (Figures 8a and 8b).

Figure 9 shows steady state results for $Ra = 2.5 \times 10^5$ for aspect ratio 1:1:1 with Pr = 10 and Pr = 0.71. The structure of the three-dimensional flow becomes complicated due to the occurrence of secondary flow. The difference in flow patterns in Figures 9a and 9b indicate that a decrease in Pr leads to an increase in advective activity. Flow patterns obtained at Pr = 100 were nearly identical to results at Pr = 10 and supports the observation made in Reference [15] that the flow becomes invariant for $Pr \geq 10$, coupled with a decrease in inertial effects.

Solutions obtained for $10^5 \leq Ra \leq 2.5 \times 10^5$ required approximately three times as much computation time as the solution for $Ra = 10^4$. Solutions attempted for $Ra \geq 10^6$ could not be achieved. This appears to be due to the inability of the finite difference mesh to adequately resolve flow variables and the inability of the coefficient matrix to maintain diagonal dominance (mesh Reynolds number ≤ 2) with central difference operators. Techniques resembling central difference accuracy but with "upwind difference" stability are discussed by Jacobs [3], Dennis and Walsh [21], and Richards and Crane [22], and can be implemented without difficulty. However, care must be taken to assure that the solutions are not overly damped; i.e., the pseudo-diffusion effect does not lead to physically unrelated solutions [8].

Bottom or Top Heating — Side Cooling

The case of bottom heating versus top heating with one vertical wall cooled (remaining walls insulated) is portrayed in steady state ω_2, Ψ_2, and θ contours in the Y = 0.5 plane in Figures 10 and 11, respectively. Results are given for $Ra = 10^4$ and 10^5. Vertical heating generally results in a stable stratification of temperature with very light recirculation (Ψ_2). In many instances, the flow field must be perturbed before a substantial horizontal (lateral) temperature gradient is created (enhancing recirculation). The cooled vertical side wall in this case acts as a temperature sink, creating a significant horizontal temperature gradient near the wall, resembling actual room heating conditions encountered in buildings.

Figure 10 appears to exhibit more comfortable (uniform) heat distribution with less circulation (minimizing drafts) than Figure 11. However, conclusions drawn from these results at low Rayleigh numbers cannot be assumed to hold for environmental heating in general. Inability of the numerical method to solve environmental heating problems where $10^6 \leq Ra \leq 10^{12}$ severely limits qualitative decisions to be made with regards to heating location. Likewise, decisions as to how the space inside the enclosure is to be used must also be considered.

The effect of increased heating is shown in Figure 12 with the Rayleigh number plotted as a function of the Nusselt number. Since the differencing scheme limited Rayleigh numbers to $Ra \leq 10^6$, the Nusselt number was calculated by the relation (at any value of Y)

$$Nu = \int_0^1 \left.\frac{\partial\theta}{\partial X}\right|_{wall} dZ \qquad (20)$$

The average value was obtained by calculating $\partial\theta/\partial x$ at X = 0,1 and computing the Nusselt number at both surfaces in the Y = 0.5 plane and averaging the results.[4] At low Rayleigh numbers, the boundary layer is thick relative to the mesh size, so that sufficient accuracy is possible by assuming only conduction and omitting convective flux. Equation (20) was thus solved with a three-point forward difference for $\partial\theta/\partial x$ and Simpson's rule for the integration. Aziz and Hellums [11] state that two-, three-, and four-point nonconserving differences for $\partial\theta/\partial x$ caused a maximum variation in Nusselt number of about 10% (less at steady state conditions). At higher Rayleigh numbers, the heat flux would more accurately be evaluated from a conservative balance.

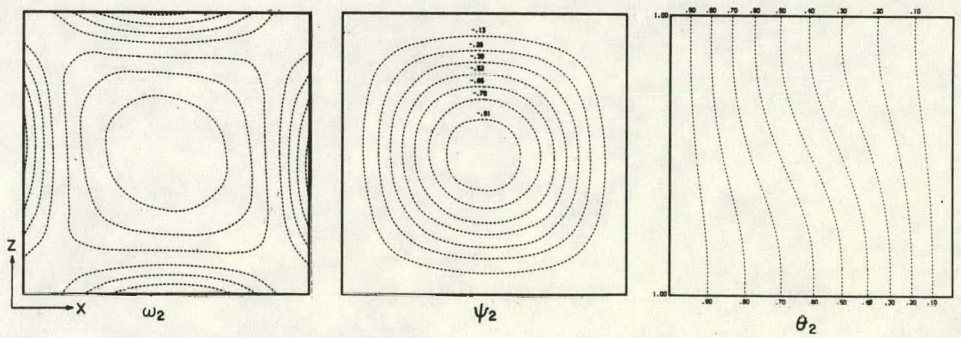

Fig. 5 ω_2, ψ_2, and 0 values for $Ra = 10^3$; Y = 0.5

[3] An effective visualization technique is the plotting of particle tracks in three-dimensional space [15]. However such methods generally require excessive computation time.

[4] For the case of comfort heating in a cubical room, $\partial\theta/\partial x$ is evaluated at X = 1 only, since all other walls are assumed adiabatic.

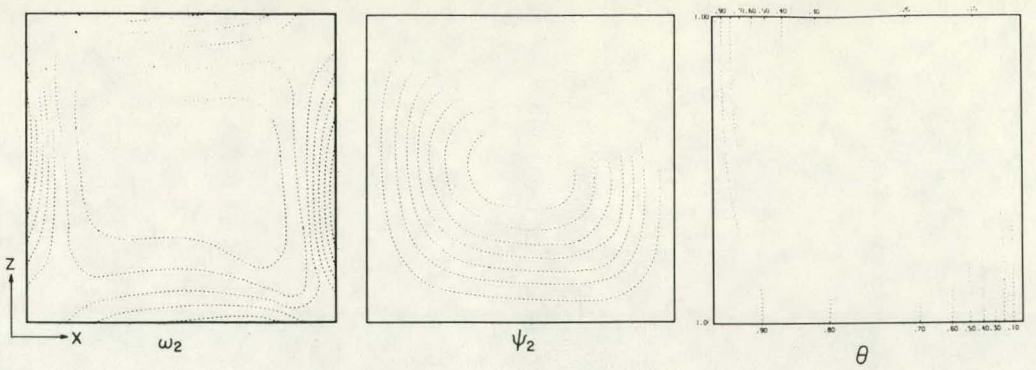

Fig. 6 ω_2, ψ_2, and θ values for Ra = 10^4; Y = 0.5

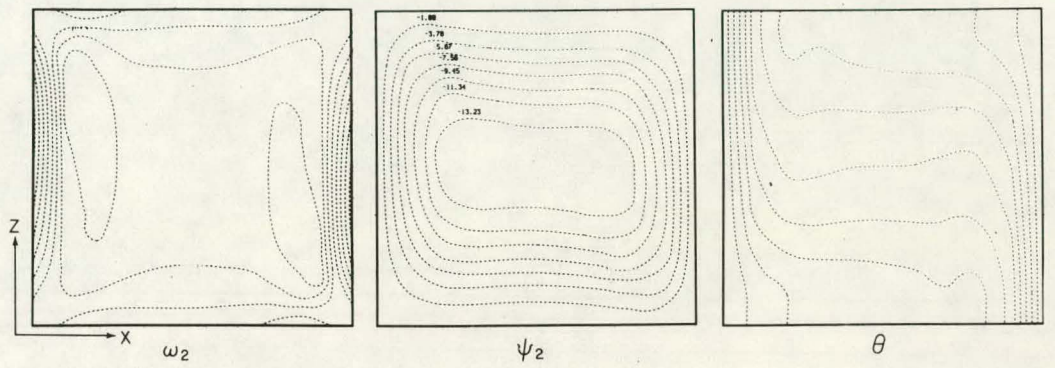

Fig. 7 ω_2, ψ_2, and θ values for Ra = 10^5; Y = 0.5

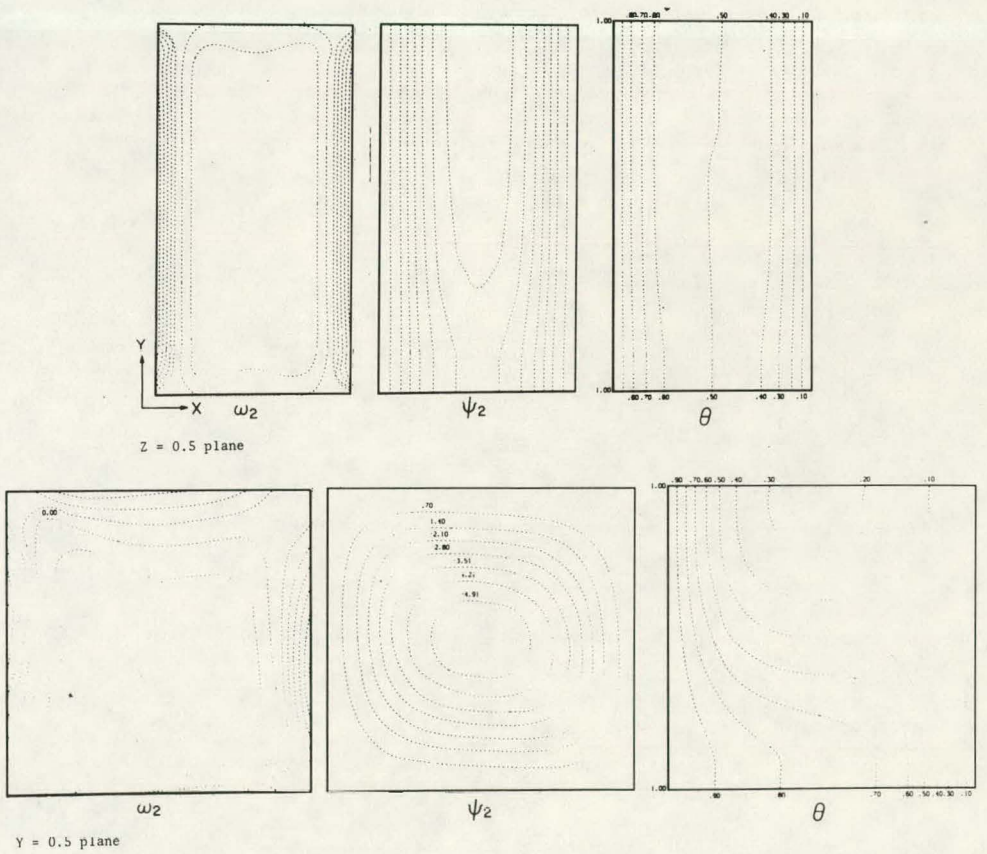

Fig 8a ω_2, ψ_2, and θ values for Ra = 10^4 (Aspect ratio 1:2:1)

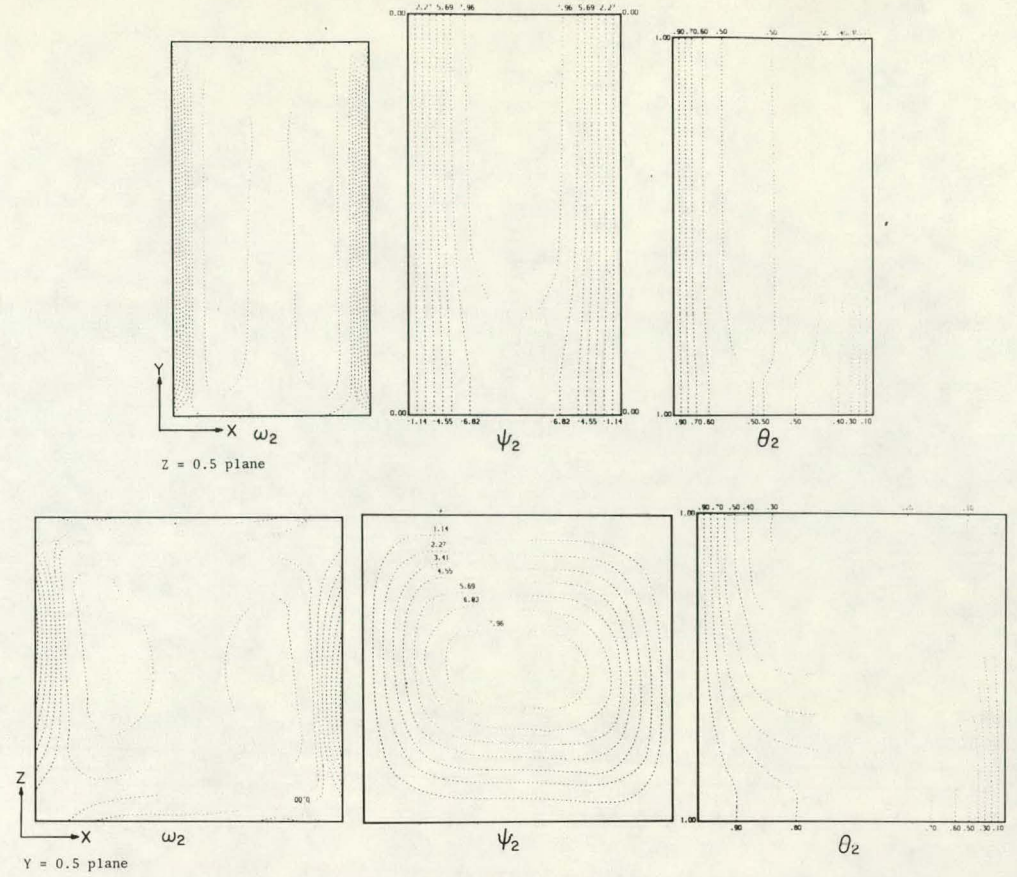

Fig. 8b ω_2, ψ_2, and θ values for Ra = 3×10^4 (Aspect ratio 1:2:1)

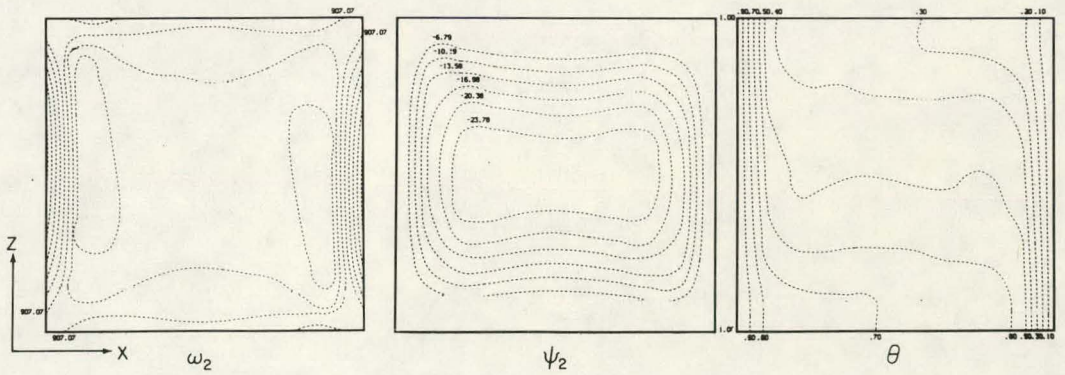

Fig. 9a ω_2, ψ_2, and θ values for Ra = 2.5×10^5; Y = 0.5; Pr = 10

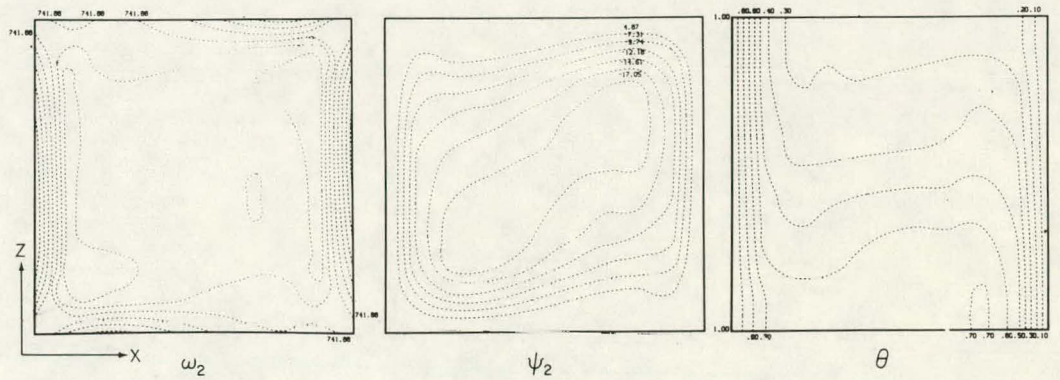

Fig. 9b ω_2, ψ_2, and θ values for Ra = 2.5×10^5; Y = 0.5; Pr = 0.71

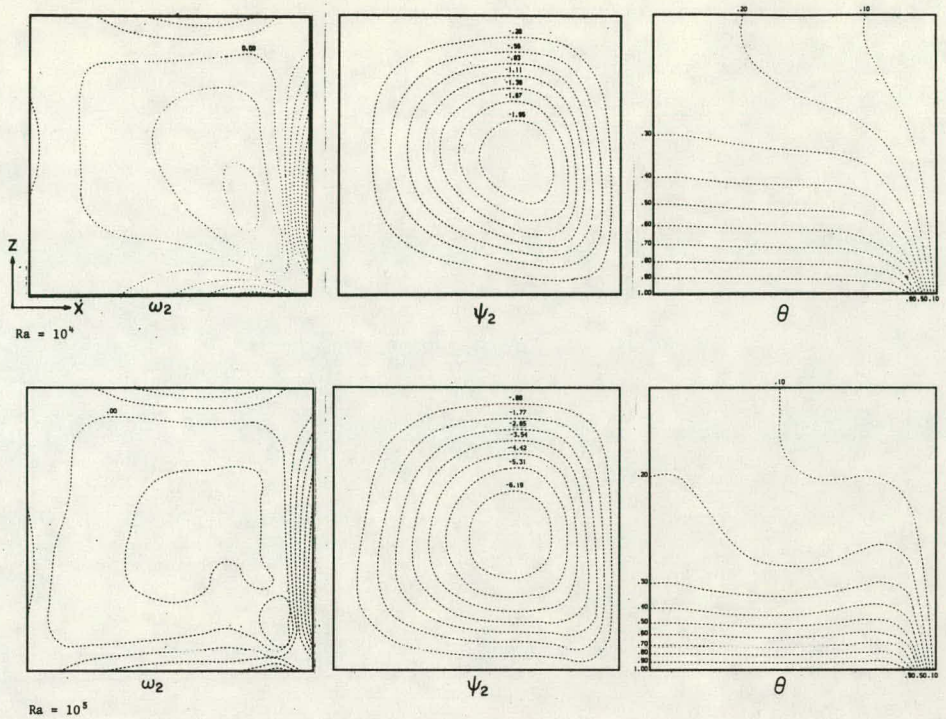

Fig. 10 Bottom heating with right vertical wall cooled
(Remaining walls insulated)

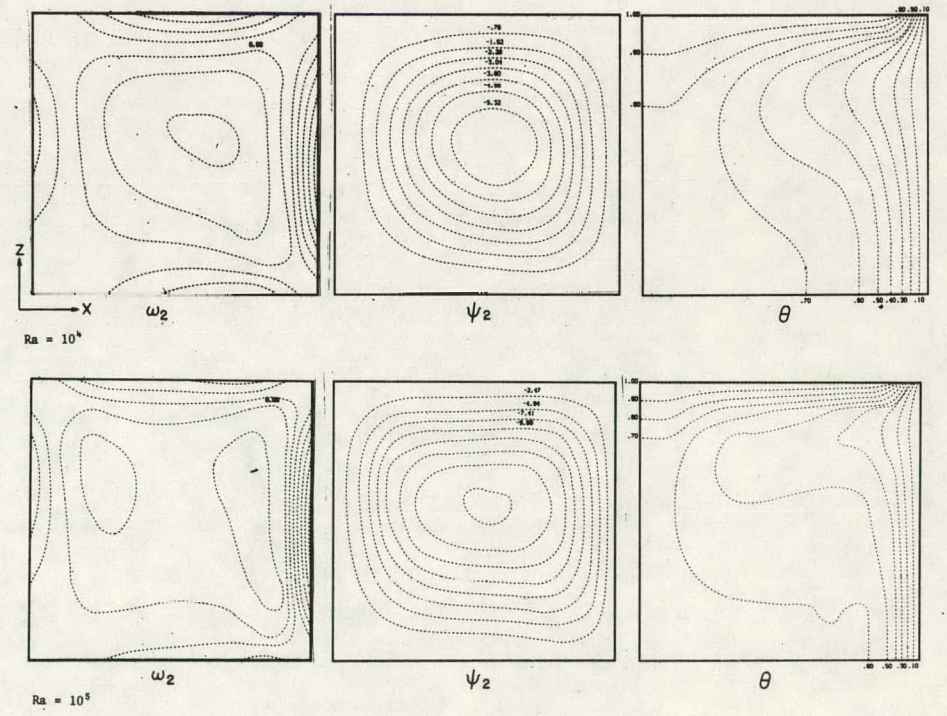

Fig. 11 Top heating with right vertical wall cooled
(Remaining walls insulated)

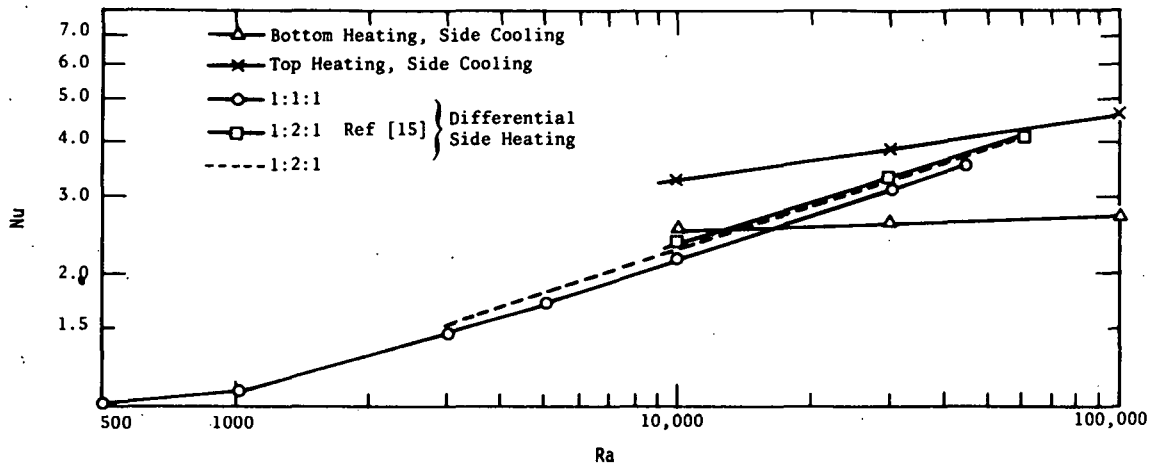

Fig. 12 Mean Nusselt number versus Rayleigh number

CONCLUSIONS

The numerical solution of three-dimensional, laminar natural convection in an enclosure has been obtained with the strongly implicit procedure (SIP). The governing equations of motion were altered to the vorticity-vector potential equation set. A false transient technique was used to enhance the convergence rate of the transient nature of the flow to steady state conditions. Although computer storage requirements are moderate, computation times are fast (usually faster than alternating direction implicit procedures). The general nature of SIP permits a wide range of problems to be solved with only minor alterations to the SIP algorithm.

Two-dimensional planar contours of flow variables obtained by SIP for the simple case of laminar natural convection due to differential side heating are similar to published results. SIP was also used to test the effectiveness of heating an enclosure from either below or above with an adjacent vertical side wall cooled. Results are inconclusive as to which form of heating is better since high Rayleigh number flows could not be obtained with the present differencing scheme.

At Rayleigh numbers on the order of 10^6 and higher, the centered differencing pattern used in SIP is unable to resolve the flow structure adequately without excessively fine mesh spacing (and subsequently small time step increment). If coarse mesh spacing is used, the solutions quickly become oscillatory and diverge. This is due to a loss of diagonal dominance in the matrix structure. Rewriting the equation set in a unidirectional discretization pattern would restore stability but reduce accuracy (with pseudo-diffusion). Higher order recursion relations, coupled with the SIP matrix algorithms, could conceivably allow higher Rayleigh number flows to be simulated.

ACKNOWLEDGMENT

The information contained in this article was developed during the course of work under Contract No. AT(07-2)-1 with the U. S. Department of Energy.

REFERENCES

1 Stone, H. L., "Iterative Solution of Implicit Approximations of Multi-dimensional Partial Differential Equations," *Society for Industrial and Applied Mathematics Journal, Numerical Analysis*, Vol. 5, No. 3, 1968, pp. 530-558.

2 Bozeman, J. D., and Dalton, C., "Numerical Study of Viscous Flow in a Cavity," *Journal of Computational Physics*, Vol. 12, 1973, pp. 348-363.

3 Jacobs, D. A. H., "A Corrected Upwind Differencing Scheme Using a Strongly Implicit Solution Procedure," *Proceedings of the International Conference on Numerical Methods in Fluid Dynamics, University of Southampton, England, Sept. 26-28, 1973*, pp. 84-98.

4 Lin, C. L., Pepper, D. W., and Lee, S. C., "Numerical Methods for Separated Flow Solutions Around a Circular Cylinder," *AIAA Journal*, Vol. 14, 1976, pp. 900-907.

5 Pepper, D. W., and Harris, S. D., "Numerical Simulation of Natural Convection in Closed Containers by a Fully Implicit Method," *Journal of Fluids Engineering*, Vol. 99, No. 4, 1977, pp. 649-656.

6 Pepper, D. W., and Harris, S. D., "Fully Implicit Algorithms for Solving Partial Differential Equations," *Journal of Fluids Engineering*, Vol. 99, No. 4, 1977, pp. 781-783.

7 Weinstein, H. G., Stone, H. L., and Kwan, T. V., "Simultaneous Solution of Multiphase Reservoir Flow Equations," *Society of Petroleum Engineering Journal*, June 1970, pp. 99-110.

8 Long, P. E., and Pepper, D. W., "A Comparison of Six Numerical Schemes for Calculating the Advection of Atmospheric Pollution," presented at the Third Symposium on Atmospheric Turbulence, Diffusion, and Air Quality, Raleigh, North Carolina, October 19-22, 1976.

9 Pepper, D. W., and Kern, C. D., "Modeling of Time-Dependent Mesoscale Concentrations," First Conference on Regional and Mesoscale Modeling, Analysis, and Prediction, Las Vegas, Nevada, May 6-9, 1975. *Bulletin of the American Meteorological Society*, Vol. 56, 1975, p. 196.

10 Ozoe, H., Yamamoto, K., Churchill, S. W., and Sayama, H., "Three-Dimensional Numerical Analysis of Laminar Natural Convection in a Confined Fluid Heated from Below," *Journal of Heat Transfer*, Vol. 98C, 1976, pp. 202-207.

11 Aziz, K., and Hellums, J. D., "Numerical Solution of the Three-Dimensional Equation of Motion for Laminar Natural Convection," *Physics of Fluids*, Vol. 10, No. 2, 1967, pp. 314-324.

12 Williams, G. P., "Numerical Integration of the Three-Dimensional Navier-Stokes Equations for Incompressible Flow," *Journal of Fluid Mechanics*, Vol. 37, 1969, pp. 727-750.

13 Holst, P. H., and Aziz, K., "Transient Three-Dimensional Natural Convection in Confined Porous Media," *Int. J. of Heat Mass Transfer*, Vol. 15, 1972, pp. 73-90.

14 Lipps, F. B., "Numerical Simulating of Three-Dimensional Bénard Convection in Air," *Journal of Fluid Mechanics*, Vol. 75, Part 1, 1976, pp. 113-148.

15 Mallinson, G. D., and de Vahl Davis, G., "Method of the False Transient for the Solution of Coupled Elliptic Equations," *Journal of Computational Physics*, Vol. 12, 1973, pp. 435-461.

16 Ozoe, H., Yamamoto, K., and Sayama, H., "Natural Convection Patterns in a Long Inclined Rectangular Box Heated from Below: Part II. Three-Dimensional Numerical Results," *Int. J. Heat Mass Transfer*, Vol. 20, 1977, pp. 131-139.

17 Hirasaki, G. J., and Hellums, J. D., "A General Formulation of the Boundary Condition on the Vector Potential in Three-Dimensional Hydrodynamics," *Quart. J. of Appl. Mathematics*, Vol. 26, No. 3, 1968, pp. 331-342.

18 Gosman, A. D., Pun, W. M., Runchal, A. K., Spalding, D. B., and Wolfshtein, M., *Heat and Mass Transfer in Recirculating Flows*, Academic Press, 1969, 260 pp.

19 Rubin, S. G., and Graves, R. A., "Viscous Flow Solution with a Cubic Spline Approximation," *Computers and Fluids*, Vol. 3, 1975, pp. 1-36.

20 Fromm, J. E., "A Numerical Method for Computing the Non-Linear, Time-Dependent, Buoyant Circulation of Air in Rooms," *Symposium on Use of Computers for Environmental Engineering Related to Buildings, Gaithersburg, Maryland, November 30 - December 2, 1970*, pp. 451-464.

21 Dennis, S. C. R., and Walsh, J. D., "Numerical Solutions for Steady Symmetric Viscous Flow Past a Parabolic Cylinder in a Uniform Stream," *Journal of Fluid Mechanics*, Vol. 50, 1971, pp. 801-814.

22 Richards, C. W., and Crane, C. M., "An Economical Central Difference Algorithm for Navier-Stokes Equations Convergent for High Mesh Reynolds Numbers," *Applied Mathematical Modelling*, Vol. 2, 1978, pp. 59-61.

NOMENCLATURE

A = coefficient for $\phi^{n+1}_{i+1,j,k-1}$

B = coefficient for $\phi^{n+1}_{i,j-1,k}$

C = coefficient for $\phi^{n+1}_{i+1,j-1,k}$

D = coefficient for $\phi^{n+1}_{i-1,j,k}$

E = coefficient for $\phi^{n+1}_{i,j,k}$

F = coefficient for $\phi^{n+1}_{i+1,j,k}$

G = coefficient for $\phi^{n+1}_{i-1,j+1,k}$

$\vec{g}$ = acceleration of gravity, $\vec{g} = g(z)$

H = coefficient for $\phi^{n+1}_{i,j+1,k}$

$\hat{i},\hat{j},\hat{k}$ = unit vector in direction of coordinate axis

L = distance between sides

$[M]$ = seven diagonal matrix of B,D,E,F,H,S,Z

$[M']$ = altered sparse matrix with 13 diagonals

P = coefficient for $\phi^{n+1}_{i,j-1,k+1}$

q = coefficient for $\phi^{n}_{i,j,k}$

R = residual, $\{R\} = [M']\{\nabla\phi^{n+1}\}$

S = coefficient for $\phi^{n+1}_{i,j,k+1}$

T = temperature

t = time

T' = coefficient for $\phi^{n+1}_{i,j+1,k-1}$

$\vec{U}$ = velocity vector

U = nondimensional velocity component in the x direction, $U = uL/\alpha$

u = velocity component in the x direction

V = nondimensional velocity component in the y direction, $V = vL/\alpha$

v = velocity component in the y direction

$\{\tilde{V}\}$ = column matrix, $\{\tilde{V}\} = [Ud]\{\Delta\phi^{n+1}\}$

W' = coefficient for $\phi^{n+1}_{i-1,j,k+1}$

W = nondimensional velocity component in the z direction, $W = wL/\alpha$

w = velocity component in the z direction

X = nondimensional horizontal coordinate, $X = x/L$

Y = nondimensional lateral coordinate, $Y = y/L$

Z = nondimensional vertical coordinate, $Z = z/L$

Z' = coefficient for $\phi^{n+1}_{i,j,k-1}$

Ld = lower diagonal matrix

Nu = Nusselt number

Pr = Prandtl number, $Pr = \nu/\alpha$

Ra = Rayleigh number, $Ra = \vec{g}\beta(T_h-T_c)L^3/\alpha\nu$

Ud = upper diagonal matrix

α = thermal diffusivity

$\alpha_1,\alpha_2,\alpha_3$ = iteration parameters

α_w,α_ψ = false transient term for $\vec{\omega},\vec{\psi}$

β = volumetric coefficient of expansion (1/T)

$\nabla = \hat{i}\,\frac{\partial}{\partial x} + \hat{j}\,\frac{\partial}{\partial y} + \hat{k}\,\frac{\partial}{\partial z}$

$\nabla^2 = \frac{\partial^2}{\partial x^2} + \frac{\partial^2}{\partial y^2} + \frac{\partial^2}{\partial z^2}$

θ = nondimensional temperature, $\theta = \frac{T-T_c}{T_h-T_c}$

ν = kinematic viscosity

τ = nondimensional time, $\tau = t\alpha/L^2$

ϕ = variable representing ω, ψ, or θ

$\vec{\psi}$ = nondimensional vector potential

$\vec{\omega}$ = nondimensional vorticity vector

ΔX = horizontal grid spacing

ΔY = lateral grid spacing

ΔZ = vertical grid spacing

$\Delta\tau$ = time step increment

$\Delta\phi^{n+1} = \phi^{n+1} - \phi^{n}$

Subscripts

i,i+1,i-1 = horizontal grid point locations

j,j+1,j-1 = lateral grid point locations

k,k+1,k-1 = vertical grid point locations

h = hot

c = cold

Superscripts

n = present time level, known values

n+1 = new time level, unknown values

Symbols

{ } = column matrix

[ ] = sparse matrix of n × m